Research in Astron. Astrophys. **2010** Vol. **10** No. **4**, 363–382
http://www.raa-journal.org *http://www.iop.org/journals/raa*

Research in Astronomy and Astrophysics

Infrared spectral evolution of carbon stars *

Pei-Sheng Chen[1], Xiao-Hong Yang[2] and Hong-Guang Shan[1]

[1] National Astronomical Observatories / Yunnan Observatory and Key Laboratory for the Structure and Evolution of Celestial Objects, Chinese Academy of Sciences, Kunming 650011, China; *iraspsc@yahoo.com.cn*
[2] Department of Physics, Chongqing University, Chongqing 400044, China

Received 2009 July 20; accepted 2009 December 17

Abstract We collected almost all Highly Processed Data Products (HPDP) of ISO SWS01 spectra for the Galactic visual carbon stars, infrared carbon stars, extreme carbon stars and carbon-rich proto-planetary nebulae (PPNs). Those infrared spectra are primarily analyzed and discussed. It is shown that either spectral shapes/peaks, or main molecular/dust features are evidenced to change in the sequence of visual carbon stars, infrared carbon stars, extreme carbon stars and carbon-rich PPNs. Statistically, in this sequence, continua are gradually changed from blue to red and locations of spectral peaks of continua are also gradually changed from short wavelengths to long wavelengths. In addition, in this sequence, intensities of main molecular/dust features are also gradually changed from prominent in the short wavelengths to prominent in the long wavelengths. Furthermore, from 2MASS and IRAS photometric data, the sequence is also proved. Results in this paper strongly support the previous suggestion for the evolution sequence of carbon-rich objects in our Galaxy, that is the sequence of visual carbon stars → infrared carbon stars → extreme carbon stars → carbon-rich PPNs.

Key words: infrared: stars — stars: carbon — stars: late type

1 INTRODUCTION

It is traditionally assumed that the spectral classes of M – S – C are an evolutionary sequence for most stars on the asymptotic giant branch (AGB) phase (Iben & Renzini 1983; Chen & Kwok 1993; Speck et al. 2005). AGB stars begin as oxygen-rich (C/O<1) stars with the spectral type of M, and as a result of carbon dredge-up from the interior, they evolve through the stage with the spectral type of S (C/O≈ 1) to carbon-rich (C/O>1) ones that are carbon stars. In the early time before the IRAS mission, the majority of carbon stars were identified by their photospheric spectra in the optical and near infrared as those called visual carbon stars (for a review see Wallerstein & Knapp 1998). After IRAS observation, the discovery that many visual carbon stars have large excesses in the far infrared (Thronson et al. 1987) has led to the theory that visual carbon stars represent an evolutionary stage just after a mass-losing episode as M stars (e.g. Willems & de Jong 1988; Chan & Kwok 1988).

After more carbon atoms have accumulated in the photosphere to form carbon-based grains, such as amorphous/graphitic carbon and silicon carbide (SiC), the stars create carbon-rich circumstellar

* Supported by the National Natural Science Foundation of China.

envelopes and then become so called infrared carbon stars. As more SiC grains are formed and the mass loss rate increases, the optical depths in the circumstellar envelopes of infrared carbon stars also increase (Chan & Kwok 1990; Speck et al. 2005). Therefore, infrared carbon stars are usually invisible in the optical and show a strong SiC emission feature at 11.2 μm in the infrared. That is why most infrared carbon stars were discovered in the infrared by IRAS observations (Little-Marenin et al. 1987; Chan & Kwok 1990; Jura & Kleinmann 1990; Chen & Chen 2003).

Furthermore, since the advent of the Two-Micron Sky Survey (Neugebauer & Leighton 1969) and the AFGL Infrared Sky Survey (Walker & Price 1975), the existence of so called extreme carbon stars has been known. Extreme carbon stars are deeply embedded in thick dusty circumstellar envelopes that efficiently obscure stars themselves at optical wavelengths and further increase the optical depths (Cohen & Schmidt 1982). Cohen (1979) suggested that extreme carbon stars are among the coolest carbon stars known. Because of very high mass loss rates with thick envelopes, in the circumstellar envelopes of extreme carbon stars, more carbon is available for dust production than for visual carbon stars and infrared carbon stars (Speck et al. 2005). Therefore, it is thought that extreme carbon stars are in the final stage of carbon-rich AGB star evolution.

At the late stage of the extreme carbon star evolution, the AGB phase ends. During this phase, the mass loss virtually stops and the circumstellar envelope begins to drift away from the central star and the star is expected to evolve into carbon-rich proto-planetary nebulae (PPNs) (Volk et al. 2000; Speck et al. 2005). Thus, the sequence of visual carbon stars $\rightarrow$ infrared carbon stars $\rightarrow$ extreme carbon stars $\rightarrow$ carbon-rich PPNs is suggested to be the evolutionary sequence in the AGB and post-AGB phases for carbon-rich objects (Chan & Kwok 1990; Volk et al. 1992; Chen & Kwok 1993; Volk et al. 2000; Speck et al. 2005).

In order to examine the evolutionary sequence of carbon-rich objects mentioned above, infrared observations, in particular, infrared spectroscopic observations are necessary because these objects emit most of their energy in the infrared region. However, before the ISO mission, spectroscopic observations in the infrared for carbon-rich objects were rare and not systematical. Thanks to the ISO mission, SWS observations in the 2–45 μm range were made for many carbon-rich objects. Thus, the systematical investigation of the infrared properties using spectral observations in the infrared for those objects becomes possible.

In this paper, almost all SWS01 observations for carbon-rich objects mentioned above are collected. Using these spectra, infrared properties and spectral features for those objects are analyzed and infrared spectral features for different kinds of carbon-rich objects are discussed. The infrared spectral feature changes linked with the evolutionary sequence mentioned above are presented.

2 WORKING SAMPLE

Firstly, it is noted that only single stars are involved in this study. Therefore, J-type carbon stars and silicate carbon stars are not included because they are in binary systems (Chen & Shan 2007 and references therein).

Secondly, samples of visual carbon stars, extreme carbon stars and carbon-rich PPNs were extracted from Bergeat et al. (2002), Chen & Shan (2007) and Szczerba et al. (2007) respectively. The sample of infrared carbon stars was extracted from Little-Marenin et al. (1987), Chan & Kwok (1990), Jura & Kleinmann (1990) and Chen & Chen (2003).

The Highly Processed Data Products (HPDP) of the ISO SWS01 observations can be extracted from Kraemer et al. (2002) and Sloan et al. (2003) for samples mentioned above. Thus, for visual carbon stars, infrared carbon stars, extreme carbon stars and carbon-rich PPNs, we obtained 19, 17, 20 and 20 HPDP SWS spectra respectively that are our working sample and listed in Table 1. In Table 1, the IRAS name, the CGCS3 number (Alksnis et al. 2001), the ISO TDT number, the IRAS LRS classification (Kwok et al. 1997) and the common name are shown for each object.

Table 1 ISO SWS Observations of Carbon Stars and Carbon-rich PPNs

IRAS	CGCS	TDT	LRS	Name
Visual Carbon Star: 19 sources				
01246–3248	234	56900115	C	R Scl
02123+1200	327	80700751	/	V Ari
03374+6229	540	64001445	C	U Cam
05028+0106	853	85801604	C	W Ori
05421+2424	1038	85403210	F	TU Tau
12226+0102	3236	21100138	C	SS Vir
12570+3805	3319	22101143	/	TT CVn
14371–6233	3516	43600471	C	[W71b]096-06
17054–4342	3773	46200878	C	Fuen C 221
17172–4020	3808	46200776	C	V1079 Sco
17419–1838	3875	86400616	C	SZ Sgr
18476–0758	4121	16401849	S	S Sct
19017–0545	4164	16402151	C	V Aql
19390+3229	4415	73600518	S	TT Cyg
19586+0922	4598	52600445	/	V1469 Aql
21168–4514	5228	37300427	S	T Ind
21358+7823	5406	56200926	C	S Cep
22036+3315	5570	20601527	C	RZ Peg
23438+0312	5928	75700419	S	TX Psc
Infrared Carbon Star: 17 sources				
01080+5327	180	62902503	C	HV Cas
02270–2619	361	82001817	C	R For
03229+4721	496	81002351	C	V384 Per
05373–0810	1017	86801101	C	V1187 Ori
06226–0905	6146	86706617	C	V636 Mon
06238+0904	1273	87102602	C	AFGL 940
12447+0425	3286	24601053	C	RU Vir
15477+3943	3652	67600104	C	V CrB
17556+5813	3921	34601702	C	T Dra
18240+2326	/	47100261	C	V1076 Her
18398–0220	4077	49901342	C	V1417 Aql
19008+0726	4162	87201221	C	V1418 Aql
19068+0544	6772	47901374	C	NETC
19321+2757	4347	52601240	C	V1965 Cyg
20396+4757	4939	08001855	C	V Cyg
21032–0024	5120	51801475	C	RV Aqr
21440+7324	5452	42602373	C	PQ Cep
Extreme Carbon Star: 20 sources				
00210+6221	6006	40401901	U	
01144+6658	6017	68800128	U	V829 Cas
02293+5748	6034	80002450	C	V596 Per
02408+5458	/	80002504	U	
03313+6058	6061	62301907	U	
06582+1507	6193	71002102	U	
09452+1330	2619	19900101	C	+10216
15194–5115	3592	29700401	C	II Lup

Table 1 — *Continued.*

IRAS	CGCS	TDT	LRS	Name
17534–3030	6690	12102004	U	RAFGL 5416
18397+1738	4078	83801219	C	V821 Her
18464–0656	6760	48300563	U	RAFGL 2256
19248+0658	4275	85800120	C	V1421 Aql
19548+3035	6851	56100849	U	RAFGL 2477
21027+5309	5131	77800722	C	V1899 Cyg
21318+5631	6888	11101103	U	RAFGL 5625
21489+5301	6893	15901205	C	
22303+5950	6906	77900836	U	
23166+1655	6913	37900867	U	RAFGL 3068
23257+1038	6916	78200523	C	IZ Peg
/	/	33800604	/	Egg Nebula
Carbon-rich PPN: 20 Sources				
01005+7910		68600302	/	
Z02229+6208		44804704	/	
04395+3601	6086	86301602	H	V353 Aur
05341+0852		69702604	/	
07134+1005	6212	72201901	U	CY CMi
13416–6243		62803904	H	
16594–4656		45800441	H	Water Lily Nebula
17297+1747	6677	81601210	C	V833 Her
17311–4924		10300636	H	Hen 3–1428
18576+0341		32401203	H	V1672 Aql
19306+1407		52501428	H	
19454+2920	6835	52601347	U	
19477+2401		18101405	U	Cloveleaf Nebula
19480+2504	6845	38300108	U	
19500–1709		14400346	H	V5112 Sgr
20000+3239	6857	18500531	U	
22272+5435		26302115	U	V354 Lac
22574+6609		39601910	U	
23304+6147		39601867	U	PN PM 2–47
23321+6545	6919	25500248	U	PN PM 2–48

From Table 1, it can be seen that most of the visual carbon stars are in Group C in the IRAS LRS at 7–23 μm indicative of the SiC feature and some are in Groups F or S indicative of the featureless or the photosphere feature; all infrared carbon stars are in Group C indicative of the SiC feature; extreme carbon stars are either in Group C indicative of the SiC feature or in Group U indicative of the flat and unusual spectrum; some of the carbon-rich PPNs are in Group U, but most are in Group H indicative of the red spectrum.

3 ANALYSES OF SWS INFRARED SPECTRA

For objects in Table 1, infrared spectra can be obtained from the Highly Processed Data Products (HPDP) of ISO SWS01 observations (Kraemer et al. 2002; Sloan et al. 2003). The spectra are plotted in Figures 1, 2, 3 and 4 for visual carbon stars, infrared carbon stars, extreme carbon stars and carbon-rich PPNs respectively. For convenience, the IRAS LRS classification is marked in the upper-left, and the IRAS name and ISO TDT are marked in the upper-right in each panel of Figures 1, 3 and 4. In Figure 2, the IRAS LRS classification is not presented because infrared carbon stars all belong to group C of the IRAS LRS.

Table 2 Equivalent Width (EW) and the Line Intensity (I in Jy) of Main Molecular/Dust Features for Visual, Infrared and Extreme Carbon Stars

Name	EW(3.05)	I (3.05)	EW(5.2)	I (5.2)	EW(11.3)	I (11.3)	EW(13.7)	I (13.7)
Visual Carbon Star								
01246–3248	0.322	–108.0	1.326	–234.7	4.334	+86.17	0.755	–3.149
02123+1200*	/	/	/	/	/	/	/	/
03374+6229	0.486	–14.07	1.407	–146.9	4.565	+84.42	0.741	–3.623
05028+0106	0.478	–33.40	1.345	–299.4	4.185	+106.7	0.717	–9.980
05421+2424	0.473	–6.022	1.387	–48.54	4.542	+24.24	0.724	–1.280
12226+0102	0.319	–66.50	1.430	–132.9	4.360	+83.55	0.785	–0.906
12570+3805*	/	/	/	/	/	/	/	/
14371–6233	0.407	–6.756	1.707	–19.99	4.144	+23.23	0.768	–0.786
17054–4342*	/	/	/	/	/	/	/	/
17172–4020	0.446	–13.89	1.436	–72.24	5.118	+83.25	0.786	–0.650
17419–1838	0.473	–3.383	1.557	–17.87	3.320	+1.579	0.814	–0.192
18476–0758	0.403	–30.26	1.326	–92.46	3.930	+17.82	0.719	–1.873
19017–0545	0.419	–71.44	1.221	–288.8	3.908	+49.39	0.715	–6.387
19390+3229	0.469	–5.107	1.342	–31.37	3.787	+4.453	0.734	–0.531
19586+0922*	/	/	/	/	/	/	/	/
21168–4514	0.469	–13.97	1.671	–7.47	3.456	+1.950	0.761	–1.211
21358+7823	0.412	–131.2	1.691	–351.3	4.348	+383.3	0.764	–11.88
22036+3315	0.352	–7.263	1.799	–7.458	3.868	+7.956	0.900	–0.885
23438+0312	0.392	–103.9	1.629	–166.5	3.508	+10.84	0.780	–1.495
Infrared Carbon Star								
01080+5327	0.413	–13.22	1.766	–36.59	4.237	+60.77	0.767	–2.153
02270–2619	0.405	–49.09	1.796	–89.98	4.319	+171.0	0.784	–2.618
03229+4721	0.412	–25.89	1.918	–36.40	4.432	+350.7	0.774	–8.417
05373–0810	0.349	–16.34	1.344	–46.67	4.021	+13.24	0.819	–0.271
06226–0905	0.426	–21.86	1.778	–54.71	4.301	+98.06	0.783	–1.665
06238+0904	0.476	–1.506	1.939	–4.625	3.991	+39.68	0.762	–2.329
12447+0425	0.414	–18.66	1.904	–22.37	4.429	+132.9	0.796	–0.661
15477+3943	0.397	–22.10	1.857	–22.77	4.601	+79.18	0.764	–1.757
17556+5813	0.409	–42.86	1.831	–68.95	4.661	+228.2	0.787	–2.157
18240+2326	0.454	–0.982	2.016	–1.241	3.768	+139.4	0.754	–17.62
18398–0220	0.396	–31.30	1.744	–108.6	3.966	+193.9	0.773	–8.903
19008+0726	0.492	–6.742	1.944	–33.40	4.182	+327.2	0.756	–16.22
19068+0544	0.385	–3.458	1.746	–11.84	4.267	+29.67	0.793	–0.320
19321+2757*	/	/	/	/	/	/	/	/
20396+4757	0.361	–101.5	1.765	–194.2	4.638	+556.2	0.773	–10.36
21032–0024*	/	/	/	/	/	/	/	/
21440+7324	0.334	–64.46	1.506	–137.3	4.217	+76.51	0.757	–2.816
Extreme Carbon Stars								
00210+6221	n	n	n	n	3.827	+7.105	0.749	–1.176
01144+6658	n	n	n	n	3.173	+14.47	0.738	–6.271
02293+5748	n	n	n	n	3.403	+0.636	0.721	–7.463
02408+5458	n	n	n	n	3.025	+1.667	0.766	–0.583
03313+6058	n	n	n	n	2.956	+1.546	0.685	–4.785
06582+1507	n	n	1.029	–0.012	3.353	+2.787	0.774	–3.964
09452+1330	n	n	n	n	3.946	+14771	0.758	–1107
15194–5115	0.353	–38.78	1.345	–42.00	3.848	+334.2	0.727	–42.61

Table 2 — *Continued.*

Name	EW(3.05)	I (3.05)	EW(5.2)	I (5.2)	EW(11.3)	I (11.3)	EW(13.7)	I (13.7)
17534–3030	n	n	n	n	3.157	+14.40	0.793	–0.820
18397+1738*	/	/	/	/	/	/	/	/
18464–0656	n	n	1.173	–2.340	3.604	+11.18	0.783	–1.162
19248+0658	0.429	–5.036	1.487	–9.642	4.506	+60.17	0.781	–0.949
19548+3035	n	n	1.334	–2.473	3.306	+6.471	0.737	–6.272
21027+5309	n	n	1.247	–1.688	4.331	+42.75	0.775	–1.337
21318+5631	n	n	n	n	2.031	+0.410	0.762	–9.482
21489+5301	n	n	1.253	–1.677	4.043	+29.92	0.756	–2.658
22303+5950	n	n	1.211	–1.334	3.301	+5.637	0.733	–5.087
23166+1655	n	n	n	n	3.163	+9.947	0.749	–27.45
23257+1038	n	n	n	n	3.874	+63.64	0.744	–7.787
Egg Nebula	n	n	n	n	3.816	+195.6	0.780	–24.09

Note: "*" indicates too noisy spectrum to give reliable results; "n," no feature detected.

At first glance, one can see that, except for some very noisy spectra, like IRAS 02123+1200, 12570+3805, 17054–4342, and 19586+0922 in Figure 1, IRAS 19321+2757, and 21032–0024 in Figure 2, IRAS 18397+1738 in Figure 3 and IRAS 05341+0852 in Figure 4, some tendencies for changes of spectral shapes and features can be found. Statistically, in the sequence of visual carbon stars, infrared carbon stars, extreme carbon stars and carbon-rich PPNs, continua are gradually changed from blue to red and locations of continuum peaks are also gradually changed from short wavelengths to long wavelengths. These tendencies indicate that color temperatures continually decrease and circumstellar envelopes gradually become thicker.

It can be seen that infrared spectral properties in the SWS are basically coincident with those in the IRAS LRS. However, when the SWS spectra are extended from 2 to 45 μm, the spectral changes become even clearer.

In addition, in this sequence, intensities of main molecular/dust features are also gradually changed from prominent in the short wavelengths to prominent in the long wavelengths. In fact, for visual carbon stars the C_2H_2+HCN feature in absorption at 3.05 μm and the C_3 feature in absorption at 5.2 μm are very strong, and the SiC feature in emission at 11.3 μm is rather strong while the C_2H_2 feature in absorption at 13.7 μm can be seen and no features at 21 and 30 μm are seen; for infrared carbon stars the C_2H_2+HCN feature in absorption at 3.05 μm is rather strong, the C_3 feature in absorption at 5.2 μm is very strong and the SiC feature in emission at 11.3 μm is very strong while the C_2H_2 feature in absorption at 13.7 μm becomes invisible and very weak features at 21μm or 30 μm are only seen in very few sources; for most extreme carbon stars the C_2H_2+HCN feature in absorption at 3.05 μm and the C_3 feature in absorption at 5.2 μm cannot be seen, and the SiC feature in emission at 11.3 μm becomes weaker while the C_2H_2 feature in absorption at 13.7 μm becomes quite strong and features at 21 and/or 30 μm are seen for some sources; for carbon-rich PPNs the C_2H_2+HCN feature in absorption at 3.05 μm and the C_3 feature in absorption at 5.2 μm are completely absent, and the SiC feature in emission at 11.3 μm becomes weak and the C_2H_2 feature in absorption at 13.7 μm is strong while the SiC feature in emission around 21μm and/or the MgS feature in emission around 30 μm become very prominent for most sources.

In order to further investigate changes for intensities of main molecular/dust features in the sequence, continua of all spectra are fitted with polynomials and all spectra are normalized. Then equivalent width (EW) and the line intensity (in Jy, positive for emission and negative for absorption) at 3.05, 5.20, 11.3 and 13.7 μm are calculated respectively. Calculated results are listed in Table 2. Note that in Table 2, results are not given for IRAS 02123+1200, 12570+3805, 17054–4342, 19586+0922, IRAS 19321+2757, 21032–0024, IRAS 18397+1738 and IRAS 05341+0852 because these spectra are too noisy to have reliable results. From Table 2 it can be found that average

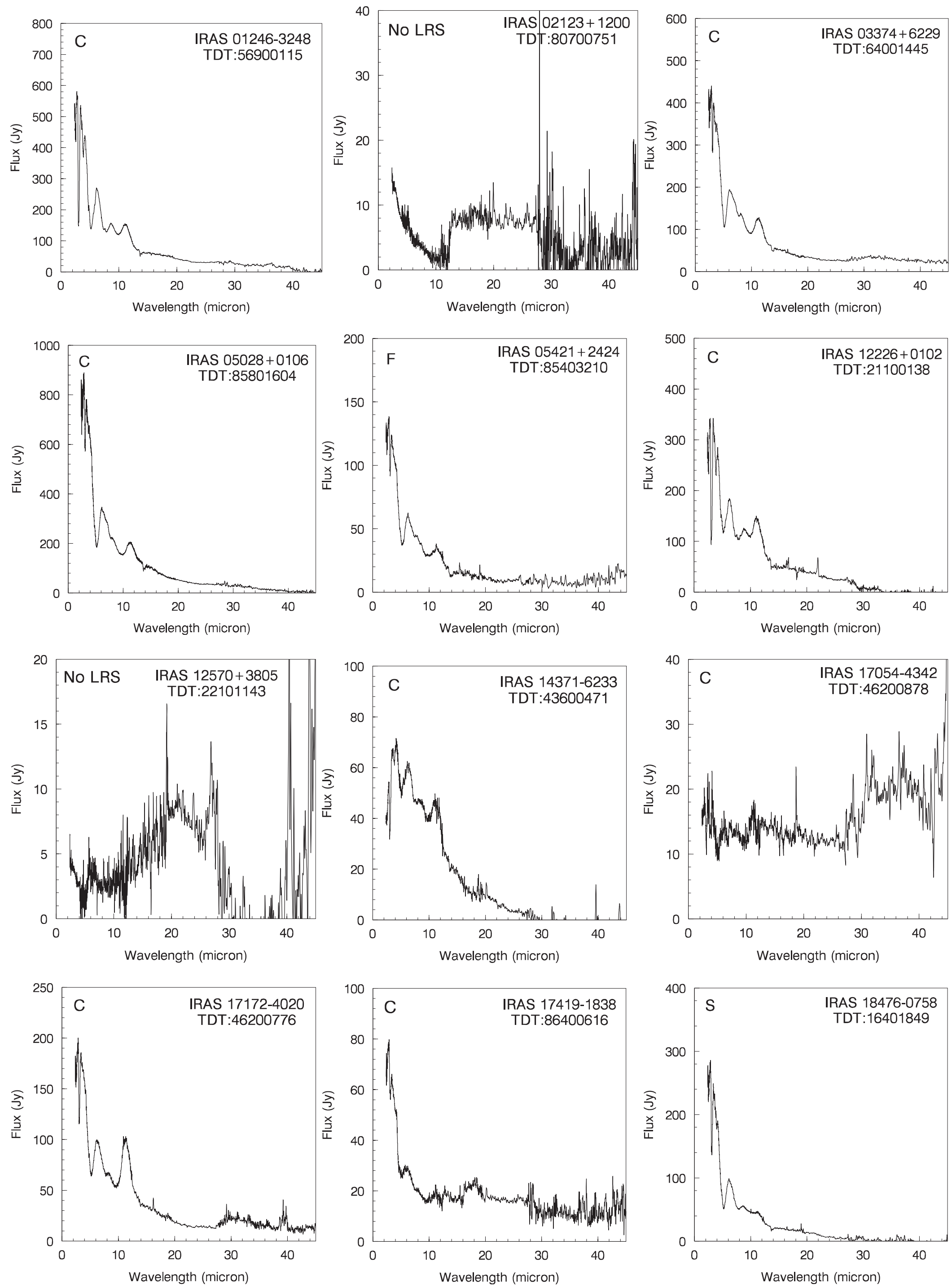

Fig. 1 ISO SWS HPDP spectra for visual carbon stars.

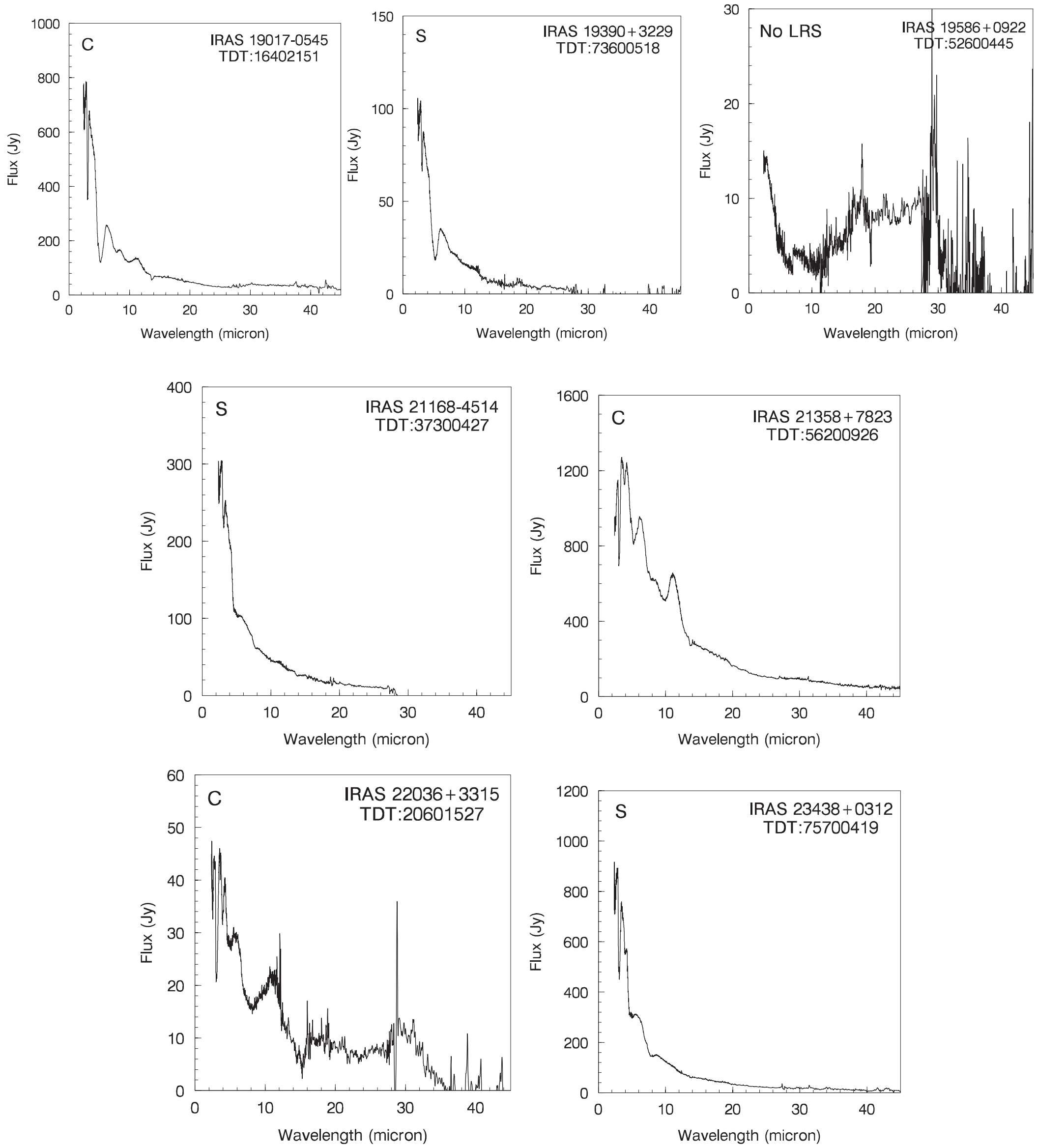

Fig. 1 — *Continued.*

EWs at 3.05 μm and at 5.2 μm are 0.421 and 1.485 for the visual carbon star, and 0.362 and 1.790 for the infrared carbon star respectively, but for extreme carbon stars these two features are only detected in a few sources; average EWs at 11.3 μm and 13.7 μm are 4.092, and 0.744 for the visual carbon stars, 4.269, and 0.753 for the infrared carbon stars and 3.510, and 0.776 for the extreme carbon stars respectively. Thus in the sequence of visual carbon stars, infrared carbon stars and extreme carbon stars, the EW of main molecular and dust features are indeed gradually changed as mentioned above.

For carbon-rich PPNs, the 21 μm SiC feature and the 30 μm MgS feature are too wide to make such calculations. Therefore, only peak wavelengths around 20–30 μm are shown. Information about

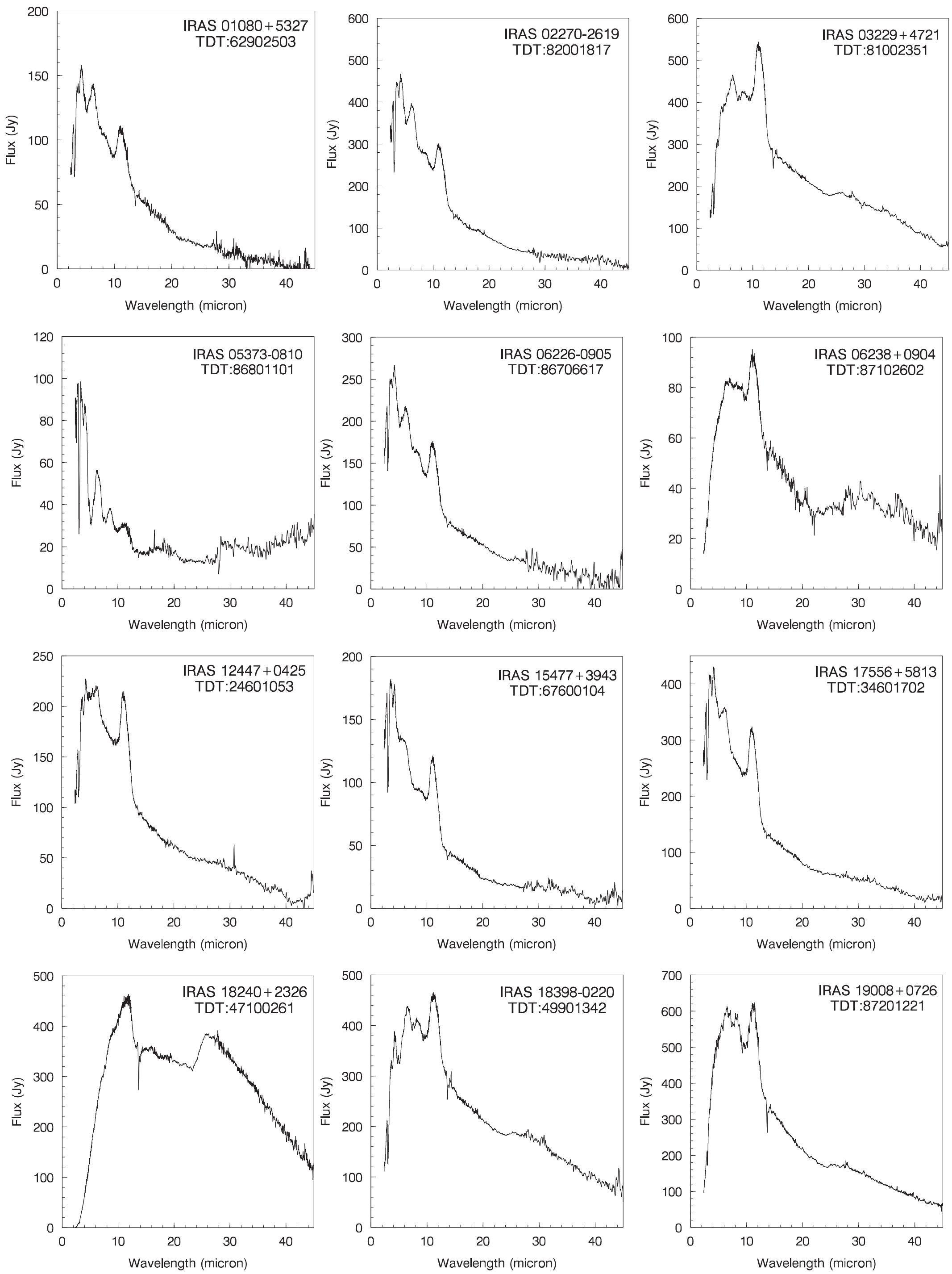

Fig. 2 ISO SWS HPDP spectra for infrared carbon stars.

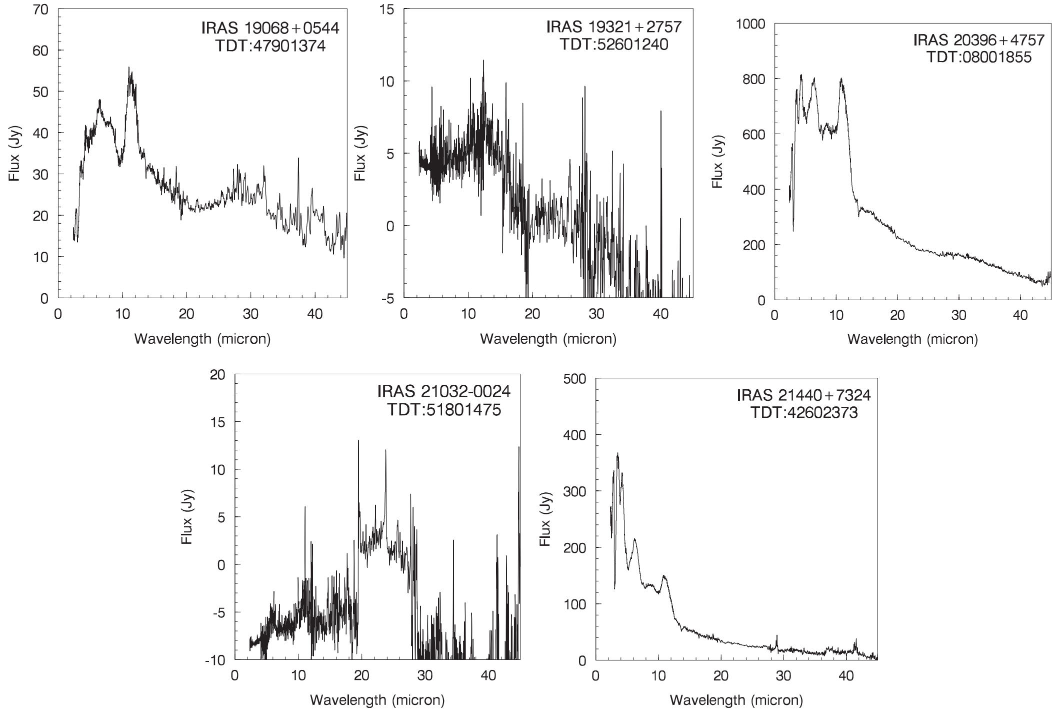

Fig. 2 — *Continued.*

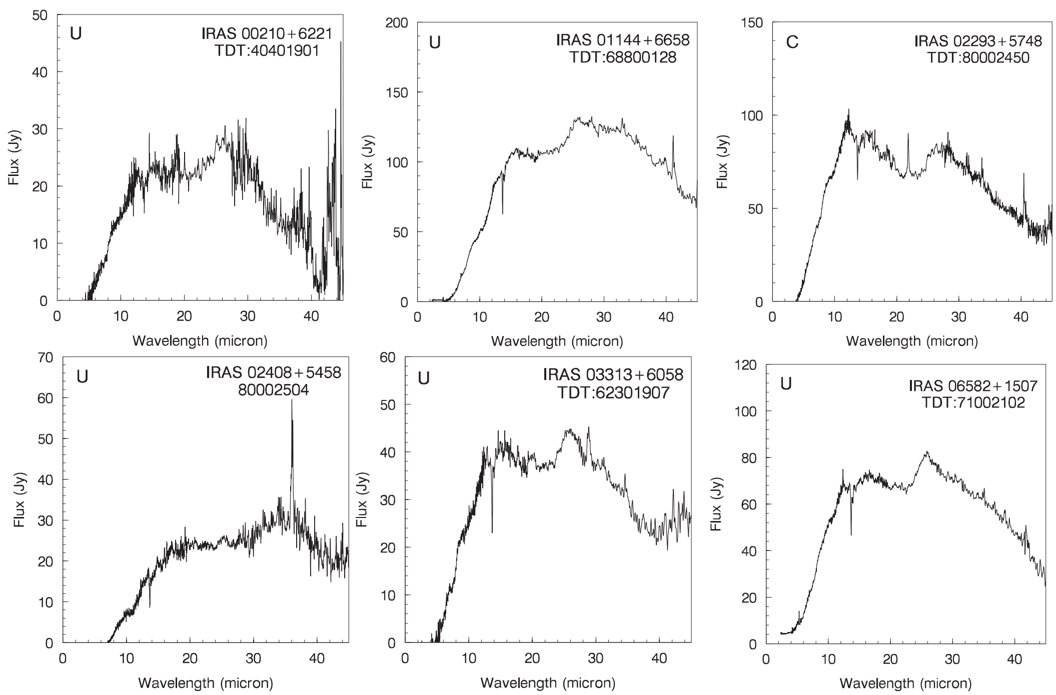

Fig. 3 ISO SWS HPDP spectra for extreme carbon stars.

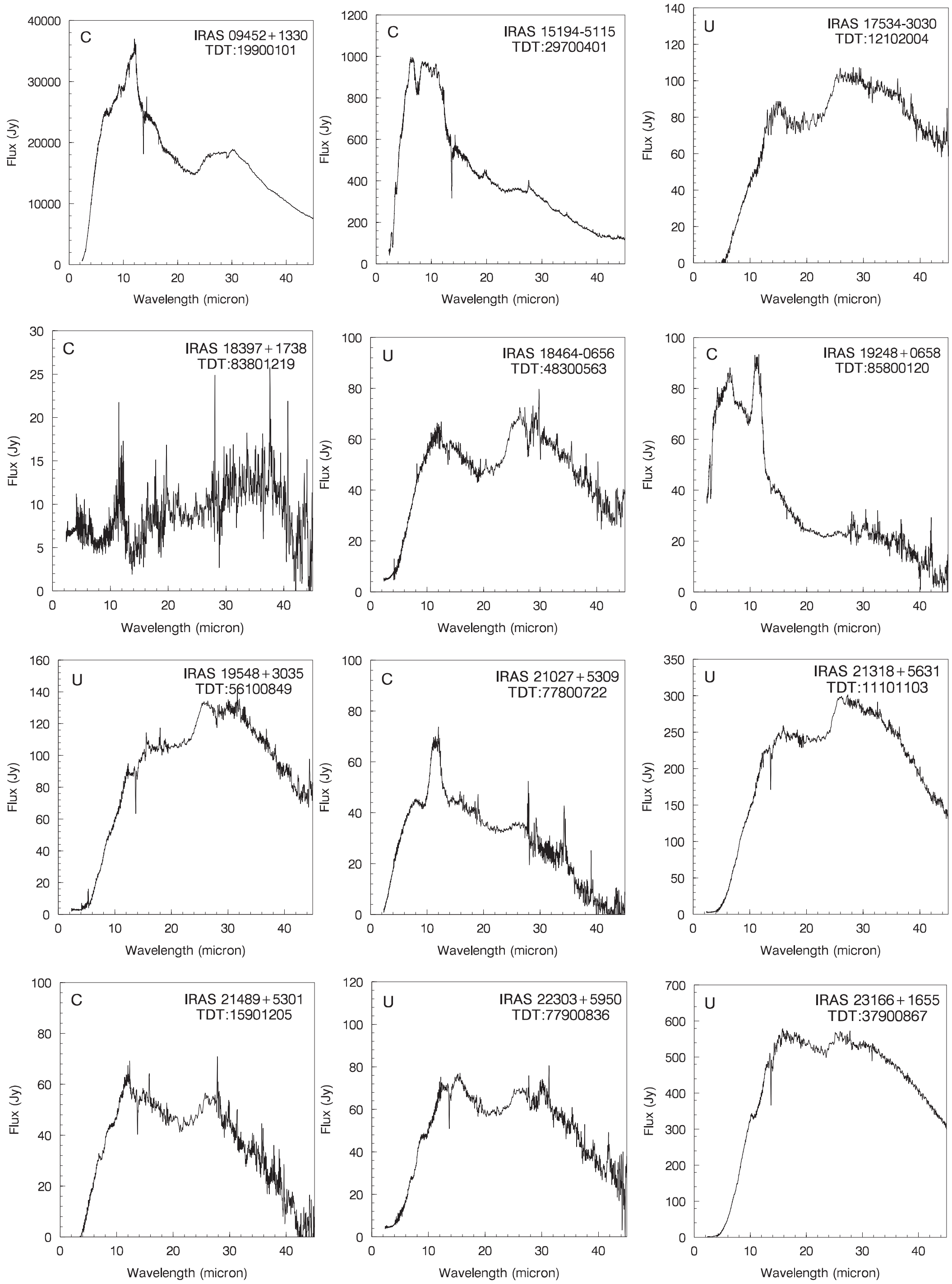

Fig. 3 — *Continued.*

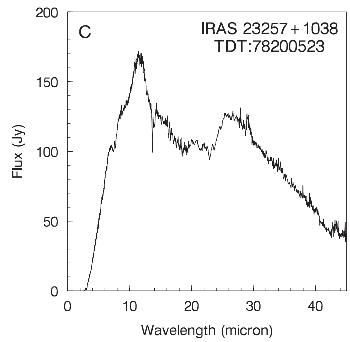

Fig. 3 — *Continued.*

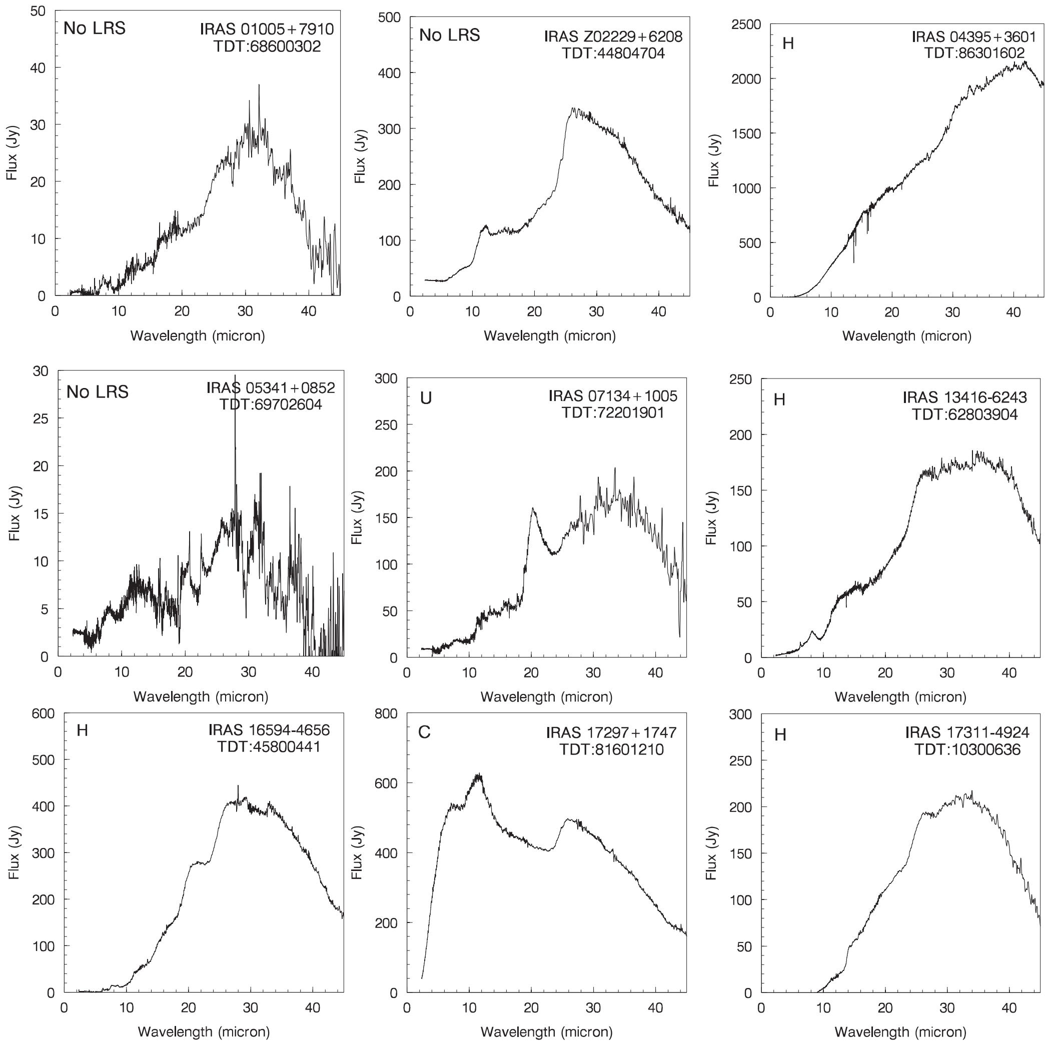

Fig. 4 ISO SWS HPDP spectra for carbon-rich PPNs.

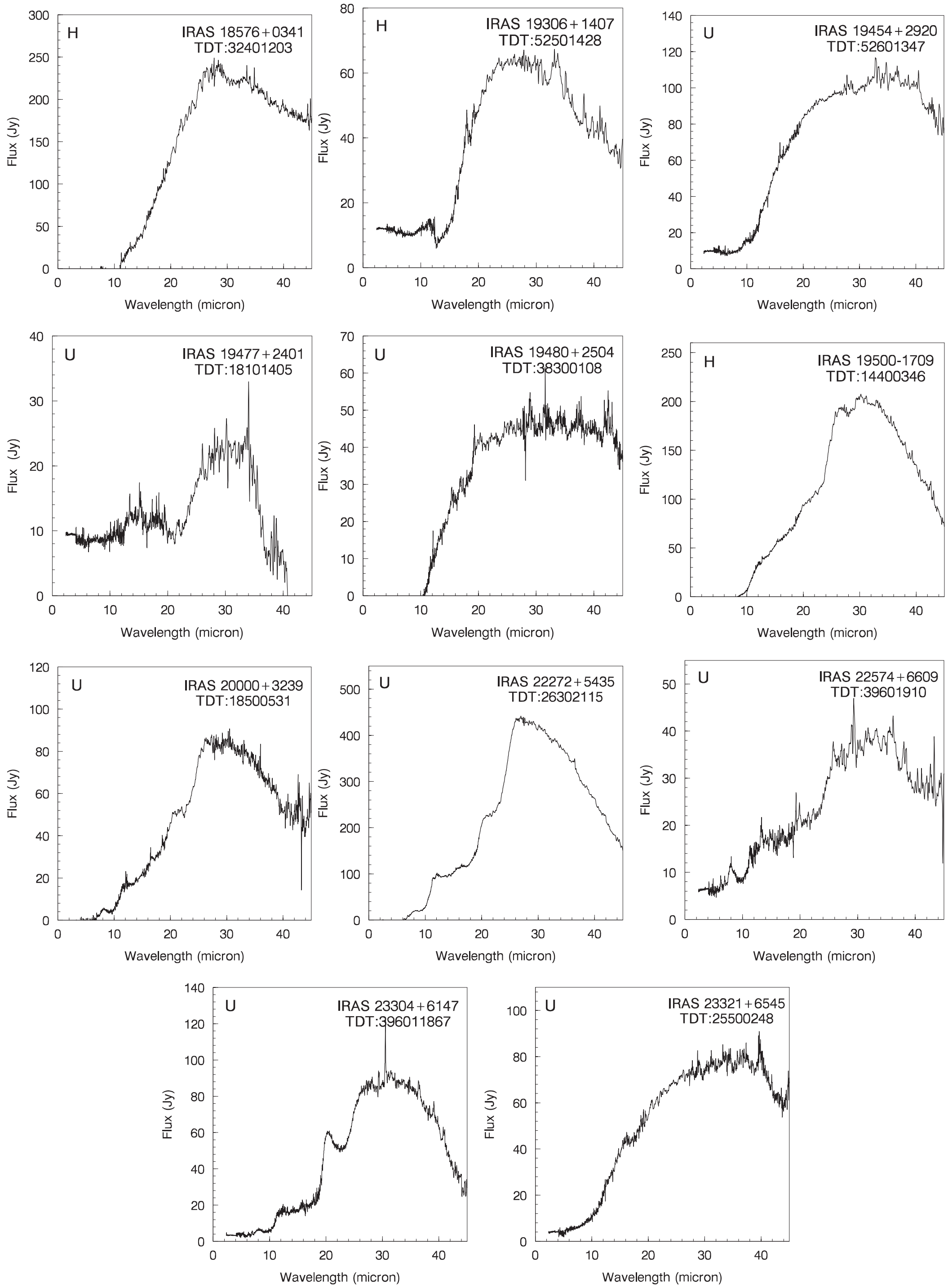

Fig. 4 — *Continued.*

Table 3 Molecular/Dust Features for Carbon-rich PPNs

IRAS Name	EW(11.3)	I (11.3)	EW(13.7)	I (13.7)	Peaked wavelength for features around 21–30 μm
01005+7910	n	n	1.032	–0.824	26, 30
Z02229+6208	n	n	0.801	–0.297	26, 30
04395+3601	3.223	+81.29	0.751	–31.31	20.2, 21.6, 30.5
05341+0852*	/	/	/	/	/
07134+1005	3.709	+11.12	0.867	–2.913	18.9, 20, 26, 30.6
13416–6243	3.982	+20.42	0.827	–1.327	26, 30
16594–4656	3.359	+42.42	0.773	–2.314	20, 26, 30
17297+1747	3.642	+131.2	0.798	–2.496	26, 31.5
17311–4924	n	n	0.815	–0.696	26, 31
18576+0341	n	n	0.616	–6.948	26, 33
19306+1407	4.255	+8.051	0.804	–0.009	19.2, 26.5, 33
19454+2920	3.028	+9.256	0.759	–1.894	27.5, 34
19477+2401	3.244	+1.737	0.837	–0.396	26–35
19480+2504	n	n	0.761	–0.788	19.3
19500–1709	3.983	+12.88	0.784	–0.848	26, 30
20000+3239	4.113	+35.89	0.943	–2.001	21, 26, 30
22272+5435	4.888	+62.28	0.828	–2.189	20.5, 26, 31
22574+6609	3.292	+1.099	0.828	–0.420	19.9, 21.2, 30
23304+6147	3.993	+7.204	0.803	–0.036	20.5, 26.5, 30
23321+6545	3.804	+5.998	0.784	–0.629	19.8, 30

Note:"*" indicates too noisy of a spectrum to give reliable results;"n," no feature detected.

carbon-rich PPNs is listed in Table 3 in which there are no data for features at the wavelengths shorter than 11.3 μm because those features are absent. From Table 3 it can be found that average EWs at 11.3 μm and 13.7 μm are 2.764 and 0.811 respectively. Compared with the visual, infrared and extreme carbon stars, for the carbon-rich PPNs the former one is the largest. It is also seen that over half of the sources have the SiC features peaking around 21 μm and almost all sources show MgS features peaking in the 26–35 μm range.

4 ANALYSES OF INFRARED PHOTOMETRIC DATA FROM 2MASS AND IRAS

In order to further understand infrared properties of carbon-rich objects, it is necessary to investigate near infrared photometric data from 2MASS and far infrared photometric data from IRAS. This is because 2MASS data mainly present properties from central stars while IRAS data reveal circumstellar phenomena in different evolutionary stages.

The original coordinates of all samples in Table 1 are from the IRAS Point Source Catalog (hereafter IRAS PSC). Although the positional error ellipses of the IRAS PSC are usually larger than 10–30 arcsec, they have a 95% confidence level (IRAS Explanatory Supplement 1988). On the other hand, the positional accuracy is about 1 arcsec in the 2MASS Point Source Catalog (2MASS Home Page, hereafter 2MASS). These two positional errors are considered for the cross-identifications of 2MASS counterparts. Thus, 71 2MASS counterparts, out of 76 samples in Table 1, were found. Among them, 62 sources have magnitudes with proper uncertainty in the JHK bands. All 2MASS counterparts are listed in Table 4. In Table 4, IRAS names with fluxes at 12, 25 and 60 μm in Jy, the 2MASS coordinates in the epoch of 2000, and magnitudes in the JHK bands are indicated. Note that magnitude uncertainties for 2MASS and flux uncertainties for IRAS are shown in brackets. If, in the bracket, no data are shown, it means the upper limiting value for the magnitude or the flux that will not be used for the following discussion.

Table 4 Molecular/Dust Features for Carbon-rich PPNs

IRAS Name	RA(2000)	Dec.	*J*	*H*	*K*	F12	F25	F60
Visual Carbon Star								
01246–3248	012658.00	–323235.8	1.973(/)	0.695(0.290)	–0.117(0.334)	162.0(6.48)	82.10(5.75)	54.80(8.22)
02123+1200	021500.09	+121423.5	5.104(0.037)	4.620(0.278)	4.364(0.282)	1.860(0.09)	0.613(0.07)	0.400(/)
03374+6229	034148.16	+623854.2	2.314(0.244)	1.063(0.154)	0.509(0.204)	121.0(4.84)	40.90(1.64)	16.90(1.52)
05028+0106	050523.71	+011039.3	1.282(0.284)	0.092(0.338)	–0.470(0.402)	184.0(7.36)	51.70(2.07)	14.90(1.28)
05421+2424	054513.73	+242512.4	3.331(0.266)	2.093(0.210)	1.574(0.220)	35.20(1.76)	9.170(0.64)	2.630(0.24)
12226+0102	122514.39	+004611.0	3.223(0.240)	1.811(0.234)	0.831(0.330)	91.60(4.58)	28.70(1.72)	5.760(0.69)
12570+3805	125922.64	+374903.6	6.265(0.024)	5.543(0.016)	5.241(0.016)	0.549(0.07)	0.250(/)	0.602(/)
14371–6233	144103.22	–624557.7	6.083(0.019)	4.158(0.172)	2.798(0.234)	47.30(1.89)	13.60(0.82)	6.570(/)
17054–4342	170906.27	–434625.2	6.129(0.021)	4.174(0.236)	3.172(0.270)	17.00(0.85)	5.080(0.36)	10.50(/)
17172–4020	172046.21	–402319.4	3.142(0.700)	1.699(0.342)	1.007(0.346)	67.80(4.07)	22.00(1.98)	3.720(0.56)
17419–1838	174456.49	–183926.4	3.907(0.272)	2.623(0.216)	2.168(0.234)	18.60(0.74)	10.00(0.70)	2.570(0.23)
18476–0758	185020.03	–075427.6	2.303(0.314)	1.140(0.262)	0.627(0.288)	65.30(5.22)	17.30(1.04)	9.280(0.84)
19017–0545	190424.16	–054105.6	1.884(0.274)	0.626(0.334)	–0.113(0.386)	150.0(6.00)	38.00(1.52)	11.40(1.03)
19390+3229	194057.01	+323705.8	3.704(0.258)	2.532(0.206)	1.960(0.226)	15.80(0.63)	4.170(0.29)	3.450(0.35)
19586+0922	200103.78	+093051.2	5.114(0.026)	4.311(0.076)	3.804(0.236)	1.900(0.11)	0.484(0.04)	0.433(/)
21168–4514	212009.48	–450118.9	1.981(0.248)	0.970(0.262)	0.564(0.316)	47.20(3.30)	13.20(0.79)	4.680(0.51)
21358+7823	213512.85	+783728.2	2.382(0.278)	1.013(0.186)	–0.029(0.192)	383.0(15.3)	133.0(5.32)	29.10(3.49)
22036+3315	220552.97	+333024.6	3.934(0.312)	2.850(0.214)	2.127(0.302)	15.70(0.94)	7.030(0.56)	1.460(0.18)
23438+0312	234623.52	+032912.2	1.197(0.242)	–0.015(0.180)	–0.508(0.248)	163.0(16.3)	39.80(2.39)	11.90(1.43)
Infrared Carbon Star								
01080+5327	011103.48	+534340.2	5.585(0.039)	3.911(0.222)	2.466(0.290)	66.90(6.02)	23.80(0.95)	5.020(0.45)
02270–2619	022915.32	–260555.9	4.230(0.274)	2.537(0.206)	1.349(0.274)	254.0(10.2)	75.30(3.77)	16.00(1.76)
03229+4721	032629.51	+473148.6	4.669(0.234)	2.596(0.192)	1.150(0.192)	535.0(58.9)	199.0(19.9)	40.00(4.00)
05373–0810	053942.62	–080908.7	4.818(0.037)	3.235(0.206)	2.241(0.248)	32.00(1.60)	8.810(0.53)	2.110(0.21)
06226–0905	062501.43	–090715.9	5.725(0.021)	3.851(0.248)	2.399(0.272)	125.0(6.25)	39.90(2.39)	9.420(0.85)
06238+0904	062637.26	+090214.9	8.613(0.026)	6.269(0.020)	4.391(0.018)	37.20(1.86)	19.20(0.96)	4.930(0.49)
12447+0425	124718.41	+040841.4	5.535(0.021)	3.940(0.076)	2.272(0.240)	230.0(11.5)	69.20(3.46)	13.70(1.64)
15477+3943	154931.31	+393417.9	3.474(0.272)	2.209(0.218)	1.321(0.276)	104.0(3.12)	32.20(1.29)	6.280(0.50)
17556+5813	175623.34	+581306.8	4.063(0.238)	2.454(0.192)	1.365(0.212)	197.0(13.8)	66.10(2.64)	15.80(0.95)
18240+2326	182605.84	+232846.7	12.641(0.029)	8.722(0.038)	5.609(0.018)	731.0(36.6)	449.0(22.5)	88.80(15.9)
18398–0220	184224.87	–021727.2	6.400(0.026)	4.100(0.182)	2.209(0.242)	560.0(145.)	245.0(31.9)	52.10(10.4)
19008+0726	190318.44	+073045.3	7.645(0.019)	5.082(0.033)	2.904(0.260)	454.0(31.8)	182.0(9.10)	37.30(4.85)
19068+0544	190915.73	+054909.8	6.856(0.018)	4.685(0.076)	3.080(0.254)	47.30(9.93)	22.10(3.32)	7.420(1.34)
19321+2757	193410.05	+280408.5	8.973(0.023)	6.180(0.020)	4.004(0.036)	325.0(35.8)	170.0(11.9)	39.00(4.29)
20396+4757	204118.27	+480828.9	3.096(0.252)	1.273(0.198)	0.117(0.192)	665.0(26.6)	234.0(11.7)	49.20(5.90)
21032–0024	210551.74	–001242.0	4.046(0.232)	2.355(0.186)	1.239(0.256)	308.0(15.4)	116.0(8.12)	22.40(2.46)
21440+7324	214428.79	+733804.8	3.444(0.240)	1.867(0.182)	0.913(0.192)	138.0(4.14)	41.70(1.25)	9.470(0.57)
Extreme Carbon Star								
00210+6221	002351.35	+623814.2	12.789(0.029)	11.862(0.030)	11.616(0.026)	48.50(1.94)	51.90(2.08)	12.50(2.00)
01144+6658	/	/	/	/	/	140.0(8.4)	206.0(8.24)	64.70(6.47)
02293+5748	023300.34	+580206.2	17.535(/)	15.894(0.159)	11.440(0.021)	173.0(5.19)	160.0(6.40)	42.20(4.64)
02408+5458	/	/	/	/	/	11.70(0.82)	20.80(0.83)	7.280(0.58)
03313+6058	033531.46	+610850.0	18.396(/)	17.688(/)	15.279(0.126)	30.90(1.55)	43.40(1.30)	15.10(1.06)
06582+1507	070108.63	+150340.8	18.592(/)	16.829(/)	14.207(0.045)	38.70(2.71)	55.50(3.89)	17.30(1.38)
09452+1330	094757.41	+131643.6	6.928(0.024)	2.839(0.184)	0.382(0.176)	47500(3800)	23100(1848)	5650.(339.)
15194–5115	152305.07	–512558.7	6.579(0.018)	4.011(0.268)	2.071(0.282)	1320.(106.)	565.0(33.9)	145.0(14.5)
17534–3030	/	/	/	/	/	196.0(27.4)	229.0(13.7)	70.60(7.06)
18397+1738	184154.54	+174108.5	5.724(0.018)	3.444(0.240)	1.744(0.230)	534.0(26.7)	239.0(11.9)	60.10(7.21)

Table 4 — *Continued.*

IRAS Name	RA(2000)	Dec.	J	H	K	F12	F25	F60
18464–0656	184910.41	–065302.8	15.781(/)	13.37 (0.050)	9.55 (0.025)	84.00(16.8)	78.90(7.89)	18.80(1.88)
19248+0658	192714.76	+070412.8	7.139(0.026)	5.148(0.069)	3.609(0.244)	94.10(3.76)	39.60(1.98)	6.320(0.69)
19548+3035	195648.45	+304402.6	15.798(0.102)	14.044(/)	13.579(/)	75.10(3.76)	109.0(5.45)	46.70(6.07)
21027+5309	210414.52	+532104.8	10.840(0.018)	8.693(0.018)	6.596(0.020)	45.50(2.73)	9.930(0.79)	8.020(/)
21318+5631	/	/	/	/	/	257.0(12.9)	312.0(12.5)	90.00(10.8)
21489+5301	215044.90	+531527.9	15.990(0.092)	11.737(0.033)	8.322(0.020)	111.0(4.44)	93.40(7.47)	26.80(2.14)
22303+5950	/	/	/	/	/	68.40(2.74)	20.40(2.24)	24.60(/)
23166+1655	231912.61	+171133.1	17.165(/)	15.402(0.113)	10.379(0.018)	707.0(35.4)	776.0(46.6)	248.0(19.8)
23257+1038	232817.11	+105437.4	14.767(0.038)	11.425(0.025)	8.408(0.021)	190.0(9.50)	142.0(7.10)	30.30(4.24)
Egg Nebula	210218.69	+364140.6	9.865(/)	9.352(0.041)	8.839(0.038)	/	/	/
Carbon-rich PPN								
01005+7910	010445.51	+792646.3	10.274(0.019)	10.017(0.030)	9.540(0.025)	3.900(0.12)	24.20(1.21)	10.10(0.71)
Z02229+6208	022641.79	+622122.0	6.723(0.021)	5.952(0.033)	5.509(0.020)	62.80(/)	208.0(/)	48.80(/)
04395+3601	044253.64	+360653.4	13.510(0.035)	11.410(0.027)	8.807(0.018)	471.0(23.6)	1110.(44.4)	1040.(52.0)
05341+0852	053655.06	+085408.7	10.009(0.023)	9.405(0.022)	9.108(0.021)	4.510(0.18)	9.850(0.69)	3.960(0.40)
07134+1005	071610.26	+095948.0	6.868(0.021)	6.708(0.036)	6.606(0.017)	24.50(1.23)	117.0(4.68)	50.10(13.0)
13416–6243	134507.25	–625816.9	10.302(0.023)	8.733(0.047)	7.505(0.029)	38.80(1.94)	121.0(6.05)	86.10(10.3)
16594–4656	170310.08	–470027.7	9.881(0.027)	9.002(0.030)	8.260(0.026)	44.90(2.25)	298.0(14.9)	131.0(22.3)
17297+1747	173155.30	+174521.0	10.536(0.023)	7.994(0.033)	5.607(0.026)	559.0(33.5)	408.0(20.4)	73.70(14.7)
17311–4924	173502.49	–492626.4	9.793(0.024)	9.543(0.027)	9.203(0.023)	18.30(0.73)	151.0(6.04)	58.70(6.46)
18576+0341	190010.89	+034547.1	12.164(0.027)	8.918(0.028)	7.007(0.020)	58.50(3.51)	425.0(21.3)	275.0(38.5)
19306+1407	193255.08	+141336.9	11.286(0.021)	10.737(0.019)	10.322(0.018)	3.580(0.21)	58.70(2.35)	31.80(2.86)
19454+2920	194724.80	+292810.8	11.853(0.031)	10.749(0.032)	10.426(0.023)	17.30(0.69)	89.60(3.58)	54.40(5.98)
19477+2401	194954.91	+240853.3	12.611(0.021)	10.752(0.019)	9.606(0.018)	11.20(0.56)	54.90(2.20)	27.10(2.98)
19480+2504	195008.27	+251200.9	15.216(0.054)	14.036(0.039)	13.559(0.049)	20.80(1.04)	67.90(2.72)	43.20(4.32)
19500–1709	195252.69	–170150.4	7.228(0.026)	6.970(0.031)	6.858(0.023)	27.80(1.67)	165.0(6.60)	73.40(8.81)
20000+3239	200159.52	+324732.9	8.021(0.020)	7.103(0.017)	6.580(0.023)	15.00(0.90)	71.00(2.84)	30.00(3.00)
22272+5435	222910.40	+545106.2	5.371(0.020)	4.894(0.029)	4.508(0.016)	73.90(2.22)	302.0(9.06)	96.60(9.66)
22574+6609	225918.36	+662548.2	14.473(0.034)	12.828(0.051)	11.546(0.031)	9.000(0.27)	29.50(1.18)	20.60(1.44)
23304+6147	233244.79	+620349.1	8.501(0.021)	7.831(0.034)	7.466(0.016)	11.40(0.68)	59.10(2.36)	26.60(2.93)
23321+6545	233422.48	+660151.7	17.515(/)	16.024(/)	15.038(0.159)	13.70(0.55)	85.60(3.42)	64.00(7.04)

For 2MASS observations in the JHK bands, Galactic interstellar extinction corrections should be made. As pointed out by Feast et al. (1982), for Galactic carbon stars there exists an approximate expression of the absolute K magnitude, $M_K = -8.0$. Therefore, for visual carbon stars, infrared carbon stars and extreme carbon stars, the Galactic interstellar extinction corrections could be made using the method from Feast et al. (1982), Chen & Chen (2003), Whitelock et al. (2006) and Chen & Shan (2007). For carbon-rich PPNs, the Galactic interstellar extinction corrections may not be made in such a way because most of their central stars are early types. Fortunately from the literature, the $E(B-V)$ or the distance can be found for all PPNs, thus Galactic interstellar extinction corrections can be obtained. The references of the $E(B-V)$ and/or the distance for all PPNs are listed in Table 5. The references for identifications of all PPNs as carbon-rich are also listed in Table 5. Note that if the obtained extinction coefficient in a certain band is smaller than the 2MASS measurement uncertainty in the same band, then the Galactic interstellar extinction correction is unnecessary. In the following discussions for all JHK magnitudes, Galactic interstellar extinction corrections were made as mentioned above.

From 2MASS observations listed in Table 4, after the Galactic interstellar extinction correction, the near infrared two-color diagram, $(H-K)$–$(J-H)$, is plotted in Figure 5 for samples

Table 5 References for Carbon-rich PPNs

IRAS	Ref. for Carbon-rich	Ref. for extinction
01005+7910	(1), (2)	(15)
Z02229+6208	(1), (2), (3), (4)	(4)
04395+3601	(14)	(16)
05341+0852	(1), (2), (5)	(17)
07134+1005	(2), (3), (4), (5), (6), (7), (14)	(5)
13416–6243	(8), (9)	(18)
16594–4656	(2)	(18)
17297+1747	(10), (14)	(19)
17311–4924	(11)	(11)
18576+0341	(1)	(20)
19306+1407	(1)	(21)
19454+2920	(14)	(22)
19477+2401	(1), (2)	(22)
19480+2504	(14)	(23)
19500–1709	(2), (12), (13)	(18)
20000+3239	(2), (3), (5), (14)	(24)
22272+5435	(2), (3), (5), (6), (13)	(18)
22574+6609	(1), (2), (3), (7)	(25)
23304+6147	(1), (3), (5), (13)	(17)
23321+6545	(14)	(23)

(1) Hrivnak et al. (2000); (2) Hrivnak et al. (2007); (3) Volk et al. (1999); (4) Hrivnak & Kwok (1999); (5) Hrivnak (1995); (6) Kwok et al. (1989); (7) Kwok et al. (1999); (8) Hony et al. (2002); (9) Sloan et al. (2007); (10) Johnson & Jones (1991); (11) Sarkar et al. (2005); (12) Clube & Gledhill (2004); (13) Hrivnak et al. (1999); (14) CGCS3; (15) Hu (2002); (16) Phillips (2004); (17) Fujii et al. (2002); (18) van der Veen et al. (1989); (19) Menzies et al. (2006); (20) Clark et al. (2003); (21) Lowe Gledhill (2007); (22) Kwok et al. (1987); (23) Neri et al. (1998); (24) Klochkova & Kipper (2006); (25) Su et al. (2001).

with good quality data from 2MASS. The black body line is also shown. From Figure 5 it is found that all carbon stars are distributed around the black body line indicative of the thermal radiation. It is also found that visual carbon stars are located in the lower-left with high color temperature, extreme carbon stars, which are located in the upper-right with low temperature and infrared carbon stars that are just between them. It is seen that most PPNs are located in the very high temperature region, and some of them are away from the black body line indicative of the influence of possible free-free and free-bound radiations from the ionized material around the central early type stars (Zhang et al. 2005). It should be noted that two objects, IRAS 04395+3601=V353 Aur and IRAS 17297+1747=V833 Her, are located in the region where extreme carbon stars are located. This implies that those two objects are very young PPNs that are just left over from the AGB phase.

From Table 4, it is found that there are 67 sources having IRAS data with good quality fluxes at 12 μm, 25 μm and 60 μm from the IRAS PSC. Following Maas et al. (2003) and Chen & Zhang (2006), those fluxes are transferred into magnitudes, thus the IRAS two-color diagram is plotted in Figure 6 for those sources. In addition, the black body line is also shown in Figure 6. Furthermore, in order to investigate the source distributions in Figure 6 in a better way, the distribution regions defined by van der Veen et al. (1988) are also shown. It is found that most visual carbon stars are located in the VIa region and to the left of the VII region which has high color temperatures. Some sources in the VIa region are believed to have infrared excess in 60 μm due to the remains of their oxygen-rich progenitors (Thronson et al. 1987; Chan & Kwok 1988). It is also found that extreme

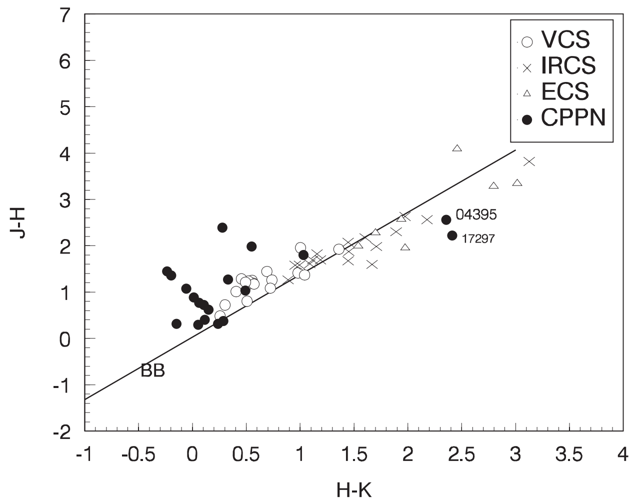

Fig. 5 Near infrared two-color diagram from 2MASS for samples in this paper.

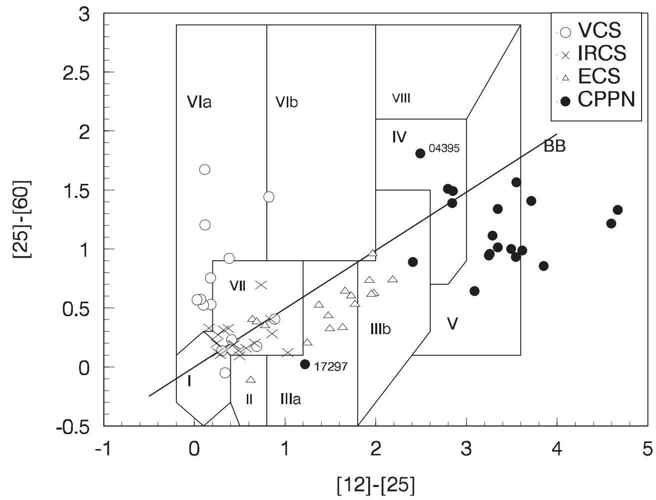

Fig. 6 Far infrared two-color diagram from IRAS for samples in this paper.

carbon stars are located in the IIIa and IIIb regions with lower color temperatures and infrared carbon stars that are located in the VII region are located just between the visual carbon stars and extreme carbon stars. In addition, PPNs are located in the IV and V regions, and even to the right of the V region, indicative of the lowest color temperatures. Distributions of samples in Figure 6 show the ideal sequence from visual carbon stars via infrared carbon stars and extreme carbon stars to PPNs. It should be noted that the location of IRAS 04395+3601 is normal for PPNs, indicative of the PPN nature while IRAS 17297+1747 is located in the IIIa region where the extreme carbon stars are located. This proves the conclusion above that it is transitioning from the AGB phase and it, as a PPN, is younger than IRAS 04395+3601.

5 SUMMARY

In this paper, almost all ISO SWS01 spectra for visual carbon stars, infrared carbon stars, extreme carbon stars and carbon-rich PPNs are presented and analyzed. It is shown that either spectral shapes/peaks, or molecular/dust features evidently change in the sequence of visual carbon stars, infrared carbon stars, extreme carbon stars and carbon-rich PPNs. Statistically, in this sequence, continua are gradually changed from blue to red and locations of spectral peaks of continua are also gradually changed from short wavelengths to long wavelengths. In addition, in this sequence, intensities of main molecular/dust features are also gradually changed from prominent in the short wavelengths to prominent in the long wavelengths. Furthermore, from 2MASS and IRAS photometric data, the sequence is also proved. Results in this paper strongly support the previous suggestion of the evolution sequence for carbon-rich objects.

Acknowledgements We are grateful to the anonymous referee for his/her fruitful suggestions. This work is supported by grants from the National Natural Science Foundation of China (Nos. 10503011, 10533050 and 10803023), the Natural Science Foundation Project of CQ CSTC (2008BB0153) and the Chinese Academy of Sciences. This work has made use of the NASA ADS database, the CDS VizieR Service, the 2MASS observation data and the ISO SWS data.

References

Alksnis, A., Balklavs, A., Dzervitis, U., Eglitis, I., Paupers, O., & Pundure, I. 2001, Baltic Astronomy, 10, 1 (CGCS3)
Bergeat, J., Knapik, A., & Rutily, B. 2002, A&A, 390, 967
Chan, S. J., & Kwok, S. 1988, ApJ, 334, 362
Chan, S. J., & Kwok, S. 1990, A&A, 237, 354
Chen, P. S., & Kwok, S. 1993, ApJ, 416, 769
Chen, P. S., & Chen, W. P. 2003, AJ, 125, 2215
Chen, P. S., & Zhang, P. 2006, ChJAA (Chin. J. Astron. Astrophys.), 6, 697
Chen, P. S., Yang, X. H., & Zhang, P. 2007, AJ, 134, 214
Chen, P. S., & Shan, H. G. 2007, Ap&SS, 312, 85
Clark, J. S., Larionov, V. M., Crowther, P. A., Egan, M. P., & Arkharov, A. 2003, A&A, 403, 653
Clube, K. L., & Gledhill, T. M. 2004, MNRAS, 355, L17
Cohen, M. 1979, MNRAS, 186, 837
Cohen, M., & Schmidt, G. D. 1982, ApJ, 259, 693
Feast, M. W., Robertson, B. S. C., Catchpole, R. M., Evans, T. L., Glass, I. S., & Carter, B. S. 1982, MNRAS, 201, 439
Fujii, T., Nakada, Y., & Parthasarathy, M. 2002, A&A, 385, 884
Hony, S., Waters, L. B. F. M., & Tielens, A. G. G. M. 2002, A&A, 390, 533
Hrivnak, B. J. 1995, ApJ, 438, 341
Hrivnak, B. J., & Kwok, S. 1999, ApJ, 513, 869
Hrivnak, B. J., Volk, K., & Kwok, S. 1999, Bulletin of the American Astronomical Society, 31, 1536
Hrivnak, B. J., Volk, K., & Kwok, S. 2000, ApJ, 535, 275
Hrivnak, B. J., Geballe, T. R., & Kwok, S. 2007, ApJ, 662, 1059
Hu, J. Y. 2002, ChJAA (Chin. J. Astron. Astrophys.), 2, 193
Iben, Jr., I., & Renzini, A. 1983, ARA&A, 21, 271
IRAS Explanatory Supplement, 1988, GPO (Washington: DC)
Johnson, J. J., & Jones, T. J. 1991, AJ, 101, 1735
Jura, M., & Kleinmann, S. G. 1990, ApJ, 364, 663
Little-Marenin, I. E., Ramsey, M. E., Stephenson, C. B., Little, S. J., & Price, S. D. 1987, AJ, 93, 663

Lowe, K. T. E., & Gledhill, T. M. 2007, MNRAS, 374, 176
Klochkova, V. G., & Kipper, T. 2006, Baltic Astronomy, 15, 395
Kraemer, K. E., Sloan, G. C., Price, S. D., & Walker, H. J. 2002, ApJS, 140, 389
Kwok, S., Boreiko, R. T., & Hrivnak, B. J. 1987, ApJ, 312, 303
Kwok, S., Volk, K., & Hrivnak, B. J. 1989, ApJ, 345, L51
Kwok, S., Volk, K., & Bidelman, W. P. 1997, ApJS, 112, 557
Kwok, S., Volk, K., & Hrivnak, B. J. 1999, A&A, 350, L35
Maas, T., Van Winckel, H., Lloyd Evans, T., Nyman, L. A., Kilkenny, D., Martinez, P., Marang, F., & van Wyk, F. 2003, A&A , 405, 271
Menzies, J. W., Feast, M. W., & Whitelock, P. A. 2006, MNRAS, 369, 783
Neri, R., Kahane, C., Lucas, R., Bujarrabal, V., & Loup, C. 1998, A&AS, 130, 1
Neugebauer, G., & Leighton, R. B. 1969, NASA Special Publication, 3047
Phillips, J. P. 2004, MNRAS, 353, 589
Sarkar, G., Parthasarathy, M., & Reddy, B. E. 2005, A&A, 431, 1007
Sloan, G. C., Kraemer, K. E., Price, S. D., & Shipman, R. F. 2003, ApJS, 147, 379
Sloan, G. C., Jura, M., Duley, W. W., Kraemer, K. E., et al. 2007, ApJ, 664, 1144
Speck, A. K., Thompson, G. D., & Hofmeister, A. M. 2005, ApJ, 634, 426
Su, K. Y. L., Hrivnak, B. J., & Kwok, S. 2001, AJ, 122, 1525
Szczerba, R., Siodmiak, N., Stasinska, G., & Borkowski, J. 2007, A&A, 469, 799
Thronson, Jr., H. A., Latter, W. B., Black, J. H., Bally, J., & Hacking, P. 1987, ApJ, 322, 770
van der Veen, W. E. C. J., & Habing, H. J. 1988, A&A, 194, 125
van der Veen, W. E. C. J., Habing, H. J., & Geballe, T. R. 1989, A&A, 226,108
Volk, K., Kwok, S., & Langill, P. P. 1992, ApJ, 391, 285
Volk, K., Kwok, S., & Hrivnak, B. J. 1999, ApJ, 516, L99
Volk, K., Xiong, G. Z., & Kwok, S. 2000, ApJ, 530, 408
Walker, R. G., & Price, S. D. 1975, AFCRL-TR-75-0373
Wallerstein, G., & Knapp, G. R. 1998, ARA&A, 36, 369
Whitelock, P. A., Feast, M. W., Marang, F., & Groenewegen, M. A. T. 2006, MNRAS, 369, 751
Willems, F. J., & de Jong, T. 1988, A&A, 196, 173
Zhang, P., Chen, P. S., & Yang, H. T. 2005, New Astronomy, 10, 325